Valero-Gómez, A.; Molina Puerto, J.; Pradas, S.; López-Tendero, MJ.; Bosch, F. (2020). Microencapsulation of cerium and its application in sol-gel coatings for the corrosion protection of aluminum alloy AA2024. Journal of Sol-Gel Science and Technology. 93(1):36-51. https://doi.org/10.1007/s10971-019-05151-8

Highlighted Manuscript

Microencapsulation of cerium and its application in sol-gel coatings for the corrosion protection of Aluminum Alloy AA2024

A. Valero-Gómez[1], J. Molina[1,2*], S. Pradas[3], M.J. López-Tendero[3], F. Bosch[1]

[1]AIDIMME. Instituto Tecnológico Metalmecánico, Mueble, Madera, Embalaje y Afines Parque Tecnológico. Avda. Leonardo Da Vinci, 38, 46980 Paterna (Valencia) Spain.

[2]Departamento de Ingeniería Química y Nuclear, Universitat Politècnica de València, Camino de Vera S/N, 46022 Valencia, Spain.

[3]Laurentia Technologies. Avda. Benjamin Franklin, 12, 46980 Paterna (Valencia) Spain.

Abstract

Cerium-containing microcapsules were obtained by means of water/oil (W/O) emulsion technology using tetraethyl orthosilicate (TEOS) as the precursor. Synthesis parameters as water/ethanol molar ratio, surfactant concentration, temperature, synthesis time, were optimized to obtain microcapsules with adequate form and size. Cerium salt is a corrosion inhibitor. Scanning electron microscopy (SEM) was employed to characterize the microcapsules and EDS and energy dispersive x-ray (EDX) microanalysis to access the encapsulated Ce. The synthesized microcapsules were incorporated in the sol-gel coating that was sprayed on AA2024 aluminum alloy. The morphology of the sol-gel coating and the distribution of the microcapsules were investigated by SEM and EDX and the corrosion resistance of the coated samples was evaluated by electrochemical impedance spectroscopy (EIS) and open circuit potential measurements. Cerium microcapsules can act as Ce nanoreservoirs blocking defects produced in the organic-

inorganic hybrid coating by precipitating Ce oxide/hydroxide and nanoloads slowing the diffusion of redox species to the aluminum surface. Higher corrosion resistance was obtained with microencapsulation of cerium than with non-encapsulated cerium.

Keywords: sol-gel, encapsulation, cerium, corrosion protection, aluminum, organic-inorganic hybrid coating

---

* Corresponding author. Fax: +34 *960915446*; telephone: +34 *961318559*

E-mail address: jmolina@aidimme.es

Conflict of interest: The authors declare that they have no conflict of interest.

1. Introduction

Corrosion produces every year a huge economic impact on metallic structures. A recent study has estimated that the global cost is around US $ 2.5 trillion per year, equivalent to 3.4 % of the Global Gross Domestic Product (GDP) [1]. In the same study, it was pointed out that by employing corrosion control practices, savings around 15-35 % could be attained. Hence, it is primordial to develop protective coatings or strategies to avoid the corrosion of metallic structures. Corrosion of metals is caused by the destructive attack caused by chemical or electrochemical reaction with the environment [2]. Different strategies have been adopted to mitigate the effects of corrosion and slow down its appearance. Among them, the use of corrosion inhibitors is remarkable [3].

Recent regulations have restricted the use of hazardous corrosion inhibitors such as chromium (VI). Hence, different environmentally-friendly alternatives have been proposed to replace this hazardous element. Natural products and extracts of different plants have been used as organic inhibitors [4-6]; however its efficiency is limited. This is the reason why organic inhibitors have been combined with inorganic inhibitors to obtain a synergistic effect [7]. Among the environmentally friendly inorganic inhibitors, rare-earth metal (REM) salts, borates, silicates and molybdates are the most used ones [8], and rare-earth metal salts (La, Ce, Nd, Pr) have shown good results. The mechanism of corrosion protection of these salts is based on the precipitation of hydroxides that hinder the diffusion of corrosive species. Cerium is the most effective one due to the low solubility of the hydroxide formed [9] and the low cost of production of cerium and lanthanum [10], making Ce the most widely used rare-earth metal salt in corrosion protection.

Organosilane coatings obtained by sol-gel methods have been also proposed as anti-corrosive coatings [11]. In this type of coatings, initially a sol is generated and grows till

a gel is obtained in the form of a 3-D material based on hydrolysis and condensation reactions of alkoxides [12]. A good fixation of the sol-gel coating on metal surface is promoted due to the binding of silanol groups of organosilanes with the hydrolyzed metal surface groups. Sol-gel coatings have been applied on different metallic substrates such as iron, aluminum, copper, zinc, or magnesium-based alloys [11]. Corrosion protection offered by sol-gel coatings is based on the barrier effect since these coatings hinder the diffusion of corrosive species [13]. However, when a defect is produced on the sol-gel coating, corrosive species can reach the metal surface. This is why anticorrosive compounds are incorporated within the sol-gel matrix [13]. A relatively new advance in corrosion protection is self-healing coatings. This type of coatings is based on the use of additives/capsules that contain a compound that is able to heal the defects or damaged areas [14]. The incorporation of cerium salts in the sol-gel matrix is among this type of coatings [14-22]. Either Ce^{3+} [16,19,20,21,22] or Ce^{4+} [15,16,17,18,20] ions have been incorporated in sol-gel coatings. The oxidation state of cerium ions can also vary during the sol-gel synthesis and thermal treatment, thus presenting a mixture of Ce^{3+} and Ce^{4+} oxidation states [19]. In all these works cerium was directly incorporated in the sol-gel matrix. Direct incorporation of additives within the sol-gel matrix has different disadvantages such as relatively rapid leaching from sol-gel matrix [23] or reaction of the inhibitor with the coating matrix. Hence, other strategies such as encapsulation technology have been used to provide a more prolonged effect and isolate the inhibitor from the coating matrix. Very little has been reported about encapsulation of cerium and incorporation in sol-gel matrices [23] or epoxy matrix [24]. The present paper aims to fill the existing gap and study the effect on incorporating cerium in the form of a salt ($Ce(NO_3)_3$) or in the form of microcapsules in a sol-gel matrix to protect aluminum against corrosion. The paper is composed of two

main parts. Firstly, the synthesis of the microcapsules of cerium by water/oil emulsion technology is optimized. Secondly, the application of the sol-gel coatings and its effects on aluminum corrosion protection is studied by means of electrochemical impedance spectroscopy (EIS) and polarization curves. The effect of encapsulated and non-encapsulated cerium on the corrosion performance of sol-gel coatings is compared.

2. Experimental

2.1. Reagents and materials

Tetraethyl ortosilicate (TEOS) (98 %) was acquired from Acrōs Organics. 3-(Trimethoxysilyl)propyl methacrylate (MAPTMS) (99,5 %) was acquired from Gelest. CH_3COOH, HCl, NH_3, NaCl and $Ce(NO_3)_3 \cdot 6H_2O$ were purchased from Merck. Sunflower Oil was employed for the synthesis of the microcapsules. Span 80 surfactant from Sigma-Aldrich was used in the synthesis of the microcapsules of cerium. Ethanol was acquired from Merck. Distilled water with a conductivity < 25 µs/cm, without chlorides and pH 5.5 was used to obtain the different sol-gel formulations. Aluminum AA2024 T3 was used as the substrate onto which the different coatings were applied by spray technique.

2.2. Synthesis of cerium nitrate microcapsules

Cerium nitrate microcapsules were obtained by water/oil emulsion technology (W/O) by varying different parameters of synthesis in order to optimize the synthesis process. Microcapsules were thereafter characterized by SEM and EDX. The optimal microcapsules obtained were thereafter added to a sol-gel formulation to obtain the sol-gel containing cerium nitrate microcapsules as explained in section 2.3. Microcapsules

were added in the end of the formulation process to minimize possible damage to the microcapsules.

Cerium nitrate microcapsules were obtained by sol-gel processes in water/oil emulsions (W/O). Microcapsules were formed using TEOS as the only organosilane. Different parameters of synthesis were studied to optimize the synthesis of the microcapsules. All synthesis were carried out at 20 ºC (since sol-gel reactions are exothermic and do not require activation) and air atmosphere. Water phase was obtained dissolving 3 g of $Ce(NO_3)_3$ into 5 mL deionized water and adding a variable amount of ethanol (water/ethanol weight proportions in grams were 5/5, 10/0 and 3/8). Span 80 surfactant was also added to the water phase (2 and 5 % in relation to the oil phase). 46 g of sunflower-seed oil were mixed with the water phase using Ultraturrax at 7000 rpm during 3 min. TEOS was used as silica precursor and incorporated through two different protocols:

- **Protocol A**. 15 mL TEOS were incorporated dropwise after the w/o emulsion was generated. In this emulsion 2% of surfactant in relation to oil and 5 g of ethanol were employed. Then 0.05 mL 2 M HCl was added dropwise and under this acid catalysis at pH 2, the emulsion was left 12 hours to complete precipitation. Formulation and quantities are shown in Table 1.

- **Protocol B**. 15 mL TEOS was added into the water phase previously acidified to pH 2 with 2 M HCl (0.05 mL) during 5 h before forming the W/O emulsions. Variable amounts of ethanol (water/ethanol weight proportions in grams were 5/5, 10/0 and 3/8), and Span 80 surfactant (2 and 5 % in relation to the oil phase) were formulated. Subsequently to emulsion formation, 2 mL NH_3 (water solution at 25 %) was added dropwise to the sol up to pH 12; under these

conditions, the gelation is immediate and produce a white precipitate. Formulations are collected in table 2.

Centrifugation was the technique selected to perform the separation of the microcapsules and was achieved at 3000 rpm during 5 minutes. The solid was washed two times with 100 mL of de-ionized water at ambient temperature. The drying temperature of the microcapsules (25°C, 40°C and 70°C) was also varied.

2.3. Pre-treatment of aluminum surface

A plasma treatment (Openair® Plasmatreater AS 400) was applied on aluminum surface to clean and activate its surface and favor the sol-gel adhesion. Plasma activation is commonly used to activate the surface of polymers [25] or textiles [26] by means of creating functional groups that enhance the adhesion of the coatings. In the field of metals, plasma techniques are used in less extension, although the increase in the surface energy of metal's surface has been demonstrated [27]. This increase of surface free energy has been attributed to chain scission of hydrocarbon contamination and metal oxide surface functionalization [27] or oxidation [28]. On top of that, with plasma methods of surface modification, water is saved when compared with conventional methods that are based on the application of different baths at elevated temperatures. Functional groups created by the pre-treatment promote the adhesion of the coating and improve mechanical and electrochemical properties of the coatings. Table 3 shows the operating parameters used to apply the plasma treatment.

The control of the surface activation was performed with an angle measuring equipment according to UNE-EN 828:2013 norm. The effect of the surface activation is usually determined by measuring the contact angle of a reference liquid on the surface of study. In this study, distilled water was used as the reference liquid. Measurements of contact

angle were taken after 30 seconds of contact between the metal surface and the drop in order to establish a comparison between the different samples. The contact angles obtained were 98° for untreated aluminum. After plasma treatment, contact angle decreased to 46° due to the formation of functional groups on metal's surface.

2.4. Sol-gel formulation

TEOS and MAPTMS were used as organosilane precursors. Regarding the preparation of the different formulations (Table 4); TEOS and MAPTMS were sequentially added to ethanol. Finally, acid water (pH 1 with acetic acid) was added till a pH of 3 was reached and hydrolysis/condensation reactions began. When needed, cerium nitrate and cerium microcapsules were added with the acidified water. The cerium content (Ce^{3+}) in the sol-gel coating was 0.5 % weight respect to the organosilanes content. The quantity of microcapsules was calculated according to its cerium content (around 5% weight average content according to EDX analyses) to have a 0.25 % of Ce. When encapsulated, cerium release is more controlled and a lower quantity of Ce is needed in order to achieve a similar effect to non-encapsulated cerium. Hence, diminishing the Ce content, an improvement of corrosion protection should be expected with encapsulated cerium. The formulation containing all the components was mixed for 30 minutes. After this time, the solution was applied on the surface of AA2024 by means of spraying technique. Coated samples were allowed to dry for 15 minutes and after this time they were dried and cured in an oven at 120 ºC for 30 minutes.

2.5. Physical and chemical characterization of the sol-gel

The size of the clusters of the sol-gel formulations with and without cerium nitrate was analyzed by means of DLS (Dynamic Light Scattering) technique with a Malvern Zetasizer equipment. The formulation containing the microcapsules was not analyzed by this technique since the sample was opaque due to the presence of cerium microcapsules. Both sol-gel formulations were also analyzed by means of FTIR-ATR (Fourier Transform Infrared Spectroscopy with Attenuated Total Reflection) with a Spectrum One FTIR spectrometer using a ZnSe crystal. Scans were performed between 4000 cm^{-1} and 650 cm^{-1}, using 3 rebounds and a resolution of 4 cm^{-1}.

2.6. Scanning electron microscopy (SEM) and Energy Dispersive X-ray (EDX)

A Jeol JSM-6300 scanning electron microscope (SEM) was used to observe the morphology and size of the cerium microcapsules obtained using an acceleration voltage of 10 kV. A Zeiss Ultra 55 field emission scanning electron microscope (FESEM) was also used to observe the distribution of the microcapsules on the sol-gel, as well as the morphology of the sol-gel coatings using an acceleration voltage of 0.5 kV. Energy dispersive X-ray (EDX) technique was used to analyze semi-quantitatively the presence of cerium in the microcapsules obtained, measurements were performed between 0 and 20 kV. Mapping of elements was also used to evaluate the spatial distribution of O, Si and Ce in the microcapsules obtained.

2.7. Electrochemical measurements

Electrochemical measurements were performed with a Zahner Zennium potentiostat/galvanostat. Electrochemical characterization of the coated samples after

exposure to corrosive medium (3.5 % NaCl) was performed by means of electrochemical impedance spectroscopy (EIS). With the EIS technique the impedance modulus |Z| and phase angle of the coatings can be measured. EIS measurements were performed within the frequency range 10^5 to 10^{-2} Hz with an amplitude perturbation potential of ± 10 mV and 8 points per frequency decade were obtained. The area of the working electrode was 10.2 cm^2. An Ag/AgCl (3.5 M KCl) reference electrode and Pt counter electrodes were used in a three-electrode configuration to perform the different measurements. Measurements were performed after 24 h exposure (to allow the system stabilization) and after 96 h exposure (were corrosion process was present). Electrochemical data was fitted to electrochemical equivalent circuit with NOVA 2.1. Software. Open circuit potential for the different coated samples was also measured after 96 h exposure to observe their tendency to corrode (nobler potentials indicate less corrosion tendency).

3. Results and discussion

3.1. Synthesis and characterization of cerium nitrate microcapsules

Scanning electron microscopy (SEM) technique was used to observe the morphology of the microcapsules of cerium obtained by varying the different parameters of synthesis and it was used to select the optimal conditions of synthesis. The different parameters varied have a marked influence on the size and morphology of the capsules obtained [29]. In the first stage of the reaction, where the W/O (water/oil) emulsion is generated, the parameters to be studied were:

- in which phase the silica precursor TEOS should be incorporated (whether in the aqueous or in the oil phase) and the type of catalyst for the sol-gel (acid or basic) [30].
- in the aqueous phase: the weight proportions between water and ethanol and the oil phase; and the concentration of the surfactant in the synthesis solution.

3.1.1. Synthesis routes

In this section, the most adequate strategy of synthesis to form the silica microcapsules on cerium nitrate salt is defined. The TEOS was selected as the source of silica to form the shell of the microcapsule through a sol-gel reaction. The addition of surfactant supports the formation of a water in oil emulsion with the water phase in the core of the micelles. The sol-gel reactions take always place in the interphase water/oil, forming the silica shell around the water core.

The two possible ways to generate the microcapsule were [29]:

- Silica precursor in the oil phase: the capsules are generated when the silica precursor TEOS in the oil phase gets in contact with the acid catalyst and a silica network precipitates on the micelle that contains the inorganic salt of cerium. 12 h of synthesis were used since the synthesis of sol-gel silica materials using acid-catalyst systems show longer gelation times than their base-catalyzed equivalents [29].

- Silica precursor in the aqueous phase: TEOS molecule is previously hydrolyzed with acid water solution and mixed with the other water phase components to form the emulsion. The capsule is formed by the migration from back to front of the hydrolyzed TEOS, and silica precipitates once in contact with the basic catalyst.

Figs. 1-a,b show the micrographs of the microcapsules obtained by means of both procedures. When TEOS is located in the oil phase and sol-gel is catalyzed by HCl, the microcapsules were not formed (Fig. 1-a). On the other hand, when TEOS is located in the aqueous phase and sol-gel is catalyzed by basic catalyst, the formation of spherical microcapsules can be clearly observed in the micrograph shown in Fig. 1-b. Table 5 shows the synthesis route and the results obtained. The influence of the pH on the formation of sol-gel has been reported [30]. In the case of acid catalysis, hydrolysis rate is larger than condensation rate and silica gels (similar to polymeric gels) are obtained [30]. Those polymeric chains disperse into the oil phase and not precipitate around the micelle containing nitrate cerium salts. In basic catalysis condensation reaction is promoted over hydrolysis one, which then favors the formation of denser colloidal silica particles around the preformed micelle [30]. The pH also affects the porosity of the microcapsules, being higher in the case of acid catalysis [29].

3.1.2. Molar ratio water/ ethanol

Different components are present in the aqueous phase: water, ethanol, surfactant and the inorganic salt to be encapsulated. The molar ratio water/ethanol is directly related with the size of the microcapsules obtained. For this reason, in the next set of experiments, only the molar ratio water/ ethanol was varied (Table 6) for the basic catalyst route. The micrographs of the microcapsules obtained using the different weight ratios are shown in Fig. 1-c,d,e. The best water:ethanol molar ratio was 2.55:1 (weight ratio 5/5 g/g) since a complete formation of the microcapsule is obtained (Fig. 1-d). When using water:ethanol molar ratio 1:1 (weight ratio 3/8 g/g) or when no ethanol is added (weight ratio 10/0 g/g) the formation of the microcapsule was not complete (Fig.

1-c and Fig. 1-e, respectively). The variation of the morphology of the microcapsules with the water:ethanol ratio can be attributed to the fact that ethanol forms hydrogen bonds with H_2O molecules, which may reduce the available free H_2O that is required for the hydrolysis of TEOS, and it is possible to control particle size by altering H_2O/ethanol ratio [31].

3.1.3. Concentration of the surfactant in the synthesis solution

For the synthesis of the microcapsules, a surfactant with a hydrophilic-lipophilic balance value around 4-6 was selected since this range is the adequate to obtain W/O emulsions. In the present study, span 80 surfactant was used, with a HLB (hydrophilic-lipophilic balance) value of 4.6. The election of the surfactant influences the morphology and size of the microcapsules [29]. Two concentrations were used, 2 and 5 % in relation to the oil weight (Table 7). In the micrographs of Fig. 2, it can be seen that the best surfactant concentration is 5 %. With this concentration, the size of the microcapsules is homogeneously distributed (Fig. 2-b). With the lowest concentration of surfactant, the size distribution is not adequate (Fig. 2-a).

3.1.4. Extraction and drying of the microcapsules

The drying temperature was optimized since this parameter influences the final aspect of the microcapsules (Table 8). Formulation B4 obtained with the basic catalyst route was selected for this study. In the micrographs of Fig. 2, it can be seen that the microcapsules dried at 25ºC are not damaged (Fig. 2-b). When using 40ºC as the drying temperature, a partial breakage of the microcapsules can be observed (Fig. 2-c). If the drying temperature is further increased till 70ºC, the breakage of the microcapsules is

total (Fig. 2-d). Hence, the optimal temperature to dry the microcapsules and to avoid damage is 25ºC.

3.1.5. EDX characterization of the microcapsules and element distribution maps

The EDX technique was used to assure the incorporation of the cerium salt within the silica microcapsules. Fig. 3 shows a micrograph of the microcapsules and the location of 4 spots where EDX analyses were performed. The EDX spectra of the different spot analyses show the presence of a peak at 4.839 keV corresponding to the spectral Kα line of Ce [32]. The other spectral line (Mα) is located at 0.884 keV but it is superposed with other spectral lines with similar energies. The table included in Fig. 3 shows the elemental composition (atomic) obtained for each of the spots analyzed. The cerium content varies between 3.36 % and 7.35 %.

Fig. 4-a shows a micrograph of the microcapsules and the element distribution maps of O (Fig. 4-b), Si (Fig. 4-c) and Ce (Fig. 4-d). These elements are components of the microcapsule; Si and O are components of the shell of the microcapsule; and Ce and O are components of $Ce(NO_3)_3$ that is incorporated inside the microcapsule. It can be seen that O distribution is majorly located where the microcapsules are present (Fig. 4-b). The location of Si is also limited to the microcapsules as can be seen in Fig. 4-c. Identically to Si, Ce is only located on the spots where the microcapsules are present. As EDX analyses, element distribution maps also confirm the incorporation of Ce within the microcapsules.

3.2. Physical, chemical and morphological characterization of the sol-gel

The physical characterization of the sol-gel formulations was performed using DLS (dynamic light scattering) technique. The stability of the sol-gel is determined by the size of the sol-gel clusters. If the size of the clusters grows rapidly, the lifetime of the sol-gel will be limited. DLS technique is very useful for this application since the size of the sol-gel clusters can be monitored with time. Fig. 5 shows the DLS spectra of the sol-gel formulations that could be measured (sol-gel and sol-gel with cerium nitrate). The DLS spectra of the sol-gel with the cerium microcapsules could not be measured since it was opaque due to the dispersion of the microcapsules. The sol-gel without additives had a mean cluster size of around 197 nm. When cerium nitrate was added to the sol-gel, the average size of the clusters increased till 230 nm. In bibliography mainly Ce^{4+} ions have been reported to increase the degree of condensation of the sol-gel [15-17,33]. The influence of Ce^{3+} on the degree of condensation is not clear and opposite results has been reported. Pausa et al. [19] reported a 3-fold increase in the viscosity of the sol-gel in the presence of Ce^{3+} and related it with the increase of reticulation. Naderi et al. [22] corroborated an increase of the condensation of the sol-gel by means of FTIR. However, the opposite effect has also been reported, where a slight decrease of condensation was observed in the presence of Ce^{3+} [34].

The physical characterization of the sol-gel formulations was also performed by means of FTIR-ATR technique. Fig. 6 shows the FTIR-ATR spectra of the sol-gel formulation with and without cerium nitrate. The FTIR spectra of TEOS and MAPTMS are quite similar due to their similar structure [35]. The most remarkable feature is the evolution of hydrolysis reaction that can be observed with the band around 3350-4000 cm^{-1}, which is attributed to hydroxyl groups [36,37]. These groups are formed by the hydrolysis reaction of alkoxides. If both spectra are compared, a higher hydrolysis extent is observed in the case of the sol-gel formulation containing cerium nitrate. This effect has

also been reported in bibliography for MAPTMS, where the decomposition of the silane chains via the methacryloxy groups was observed [36]. The increased reactivity of TEOS in the presence of Ce^{3+} has also been reported [38]. However, an increase in the intensity of the band of Si-O-Si at around 1050-1150 cm^{-1} that indicates condensation [22] was not clearly observed and similar transmittance was obtained for both samples. The ratio between the transmittance intensity of Si-OH and Si-O-Si bands was calculated for both samples, obtaining a value of 5.01 and 3.07 for sol-gel without and with Ce^{3+}, respectively. This indicates a higher hydrolysis degree in the case of the sol-gel containing Ce^{3+}. The higher hydrolysis degree in the case of Ce^{3+}-containing sol-gel could explain the slight increase of the clusters size observed by DLS technique.

The morphology of the sol-gel coatings was observed by means of FESEM technique. Fig. 7-a shows that the sol-gel coating without additives is smooth and only some cracks can be observed on the surface of the coatings, probably caused during the cutting of the metal piece or the thermal treatment. The formation of cracks during the thermal treatment is normal above a certain thickness due to the residual stresses accumulated [39]. The addition of cerium had no influence on the morphology of the coating and a smooth sol-gel coating was obtained, although the presence of more cracks could be observed (Fig. 7-b). Fig. 7-c,d show the morphology of the sol-gel coating when the cerium microcapsules were added to the sol-gel formulation. The presence of the microcapsules can be easily observed inside the sol-gel coating, since the protuberances caused by the microcapsules can be easily seen on the surface of the coating. These micrographs corroborate the incorporation of the microcapsules inside the sol-gel coating. Some cracks could also be observed due to the reason explained previously; in this case the extent of the cracks was higher than in the case of the sol-gel without additives.

An EDX characterization was also performed for the different samples in zones that had been in contact with NaCl for 96 h and in zones where the coating was not in direct contact with NaCl solution (surrounding zone of the one in contact with NaCl solution). Figure 8 shows the EDX characterization of the sample coated with the SGA sol-gel. In the upper micrograph, the zone that was not in contact with the NaCl solution is presented. On the other hand, in the lower micrograph a zone in contact with salt solution is presented. Cu, Mn and Mg are sometimes detected in the EDX analyses since they are present in the composition of the AA2024 alloy. In the zone that was not in direct contact with NaCl solution, Cl is detected, although not Na. This could be due to migration of Cl (since both zones are separated only by some millimeters) or by contamination, since Al was not present in significant quantities. The effect of the corrosion process can be clearly appreciated in the comparison of both EDX spectra. The most remarkable feature is the increase of the intensity of Al band in the zone with exposure to NaCl solution due to the corrosion process.

Figure 9 shows the EDX characterization of the sample coated with the SGA + Ce sol-gel. In the lower part of the micrograph, an analysis of the coating which is not in direct contact with the NaCl solution is presented. In the upper part of the micrograph, an analysis of the sol-gel exposed to NaCl can be observed. In both cases, the presence of different bands attributed to Ce can be observed in the spectra; which confirmed the incorporation of Ce to the coating. In this sample, an increase of the Al content was also observed in the zones that had been in contact with NaCl solution, which was attributed to the corrosion process of Al alloy.

Figure 10 shows the EDX characterization of the sample coated with the SGA + Ce microcapsules sol-gel in a zone that was not exposed to NaCl solution. The EDX characterization was performed in a zone with presence of microcapsules and in another

zone without microcapsules. The EDX spectra obtained were similar in both cases. The presence of Al is minimal in both cases, which indicates a good coverage of the AA2024 sample. However, when the SGA + Ce microcapsules sol-gel coated sample was exposed to NaCl solution; the performance of the coating was different, depending on the presence of Ce microcapsules or not (Figure 11). In the zones with the presence of microcapsules, the presence of Al was much lower than in the zone without the microcapsules. This indicates that corrosion begins preferentially in the zones where Ce microcapsules are not present since microcapsules increase the diffusion path length of corrosive species, thus difficultating the corrosion process.

3.3. Electrochemical characterization of the coatings

3.3.1. Electrochemical impedance spectroscopy

Electrochemical impedance spectroscopy (EIS) technique was used to characterize the corrosion resistance of the coatings and is widely used in the analysis of anticorrosive coatings [40].

In Fig. 12 the EIS data as well as the fitted response according to electrochemical equivalent circuits is presented. Fig. 12-a shows the Bode plots for the impedance modulus for the different AA2024 coated samples after 24 h and 96 h of exposure to 3.5 % NaCl (corrosive media). After 24 h of exposure to corrosive media, the lowest impedance modulus (|Z|) at 0.01 Hz was obtained for the bare AA2024 sample, which indicates the lowest resistance to corrosion. When comparing the effect of encapsulated and non-encapsulated cerium, encapsulated cerium produced coatings with higher impedance modulus than non-encapsulated cerium. The highest impedance modulus

was obtained for the AA2024 treated with plasma and coated with the sol-gel; although the sol-gel containing the cerium microcapsules had a similar value of |Z| at 0.01 Hz. Table 9 shows the values of |Z| at 0.01 Hz for the different samples after 24 h and 96 h of exposure to 3.5 % NaCl. After 96 h of exposure a slight decrease of the impedance modulus could be observed specially at intermediate frequencies.

Fig. 12-b shows the bode plots for the phase angle of the different samples analyzed. The EIS characterization of aluminum in 3.5 % NaCl solution showed two time constants, data was fitted according to the electrochemical equivalent circuit presented in Fig. 13-a. The first one corresponds to the layer of alumina that is formed on aluminum surface and appeared at frequencies around 10 Hz. The second time constant at frequencies below 10^{-1} Hz corresponds to the electron charge transfer process from corrosion of aluminum [21].

When the sol-gel layer was deposited on AA2024, the first time constant corresponds to the sol-gel layer, the second one to the oxides layer and the third one to the corrosion process. The electrochemical equivalent circuits used to fit data are presented in Fig. 13-b (circuit with two time constants that is used when corrosion is not observed) and Fig. 13-c (circuit with three time constants that is used when corrosion is observed). The sol-gel layer is responsible for the increase of the impedance modulus at 0.01 Hz. This increase is higher in the case of using encapsulated cerium when compared with non-encapsulated cerium. The values of the fitted parameters according to electrochemical equivalent circuits presented in Fig. 13 are presented in Table 10. After 24h and 96 h exposure to NaCl 3.5 %, the highest electrical resistance (R1) of the sol-gel coating was obtained for the s-g Ce cap coating as can be seen in Table 10. For example, after 96 h exposure to NaCl 3.5 %, the electrical resistance of the sol-gel coatings was 28.6, 6.5

and 127 kΩ for s-g, s-g Ce and s-g Ce cap coatings, respectively. This demonstrates the superior performance of using encapsulated cerium rather than non-encapsulated cerium. The time constant corresponding to the corrosion process was present for all samples at 96 h. After 24 h the time constant corresponding to the corrosion process was not present in the samples coated with the sol-gel and the sol-gel containing Ce microcapsules. In the case of the sol-gel containing non-encapsulated Ce, this process was observed after 24 h exposure to corrosive media. This also proves the superior performance of Ce microcapsules when compared with Ce directly incorporated in the sol-gel matrix.

Values of open circuit potential after 96 h exposure were also taken as an indication of the tendency to corrode. The highest open circuit potential values were obtained for the sample coated with sol-gel coating and the sol-gel coating containing the cerium microcapsules (-0.38 V) which denotes the most noble behavior among the different samples. When non-encapsulated cerium was incorporated, open circuit potential lowered to -0.439 V. Finally, bare aluminum presented an open circuit potential of -0.53 V.

Encapsulated cerium provides a better protection than cerium directly added to the sol-gel matrix, although the content of cerium in the formulation containing the microcapsules was half the content of cerium of the formulation containing cerium directly added to the sol-gel matrix. Cerium directly added to the sol-gel coating has the disadvantage of rapid leakage [41], drawback that is avoided with microencapsulation of cerium. On top of that, cerium microcapsules increase the diffusion length of corrosive species, thus decreasing the corrosion rate. This effect has also been reported for other type of particles included in the sol-gel such as graphene oxide [42,43], clay [44], etc. In addition, the sol-gel formulation containing the cerium microcapsules also

presents the most positive open circuit potential (most noble behavior) after 96 h of exposure to corrosive medium.

3. Conclusions

Encapsulation of cerium nitrate by tetraethyl orthosilicate (TEOS) has been achieved by water/oil emulsion technology. Among the different conditions of synthesis tested, the best appearance of the microcapsules (as observed by SEM) was obtained when TEOS was placed in the aqueous phase; a weight ratio (H_2O:EtOH) 1:1; a weight ratio (oil:dispersant) 20:1; basic catalysist (NH_3 25 % weight) and a drying temperature of 25ºC were used. Energy dispersive X-ray analyses and element distribution maps confirmed the incorporation of cerium within the microcapsules.

When incorporated in a sol-gel formulation as anticorrosive additive, cerium microcapsules showed a better performance than non-encapsulated cerium. Higher values of impedance modulus ($|Z|$) and higher values of open circuit potential were observed after 96 h of exposure of the probes to 3.5 % NaCl in the case of encapsulated cerium nitrate. Direct addition of cerium has the drawback of rapid leakage; encapsulation prolongs the cerium effect in the sol-gel matrix. In addition, cerium microcapsules increase the diffusion path length of corrosive species, thus increasing the corrosion resistance of the coatings. With half of the content of cerium when compared with direct addition of cerium to the sol-gel, cerium microcapsules achieved better anticorrosive performance.

Acknowledgements

Authors wish to thank to the Instituto Valenciano de Competitividad Empresarial (IVACE) (project reference IMAMCC/2016/1) for the financial support. Electron Microscopy Service of the UPV (Universitat Politècnica de València) is gratefully acknowledged for help with FESEM and EDX characterization.

References:

[1] Nace International, International measures of prevention, application, and economics of corrosion technology study (2016). http://impact.nace.org/documents/Nace-International-Report.pdf. Accessed 12 April 2019.

[2] Yadla SV, Sridevi V, Lakshmi MVVC, Kumari SPK (2012). A review on corrosion of metals and protection. Int J Eng Sci Adv Tech 2:637-644.

[3] Dariva CG, Galio AF (2014) In: Aliofkhazraei M (ed) Developments in Corrosion Protection, InTech.

[4] Rani BEA, Basu BBJ (2012) Green Inhibitors for Corrosion Protection of Metals and Alloys: An Overview. Int J Corr :Article ID 380217.

[5] Gece G (2012) Drugs: A review of promising novel corrosion inhibitors. Corros Sci 53:3873-3898.

[6] Raja PB, Sethuraman MG (2008) Natural products as corrosion inhibitor for metals in corrosive media - A review. Mater Lett 62:113-116.

[7] Umoren SA, Solomon MM (2017) Synergistic corrosion inhibition effect of metal cations and mixtures of organic compounds: A Review. J Environ Chem Eng 5:246-273.

Figure 1

Click here to access/download;Figure;Figure 1.tif

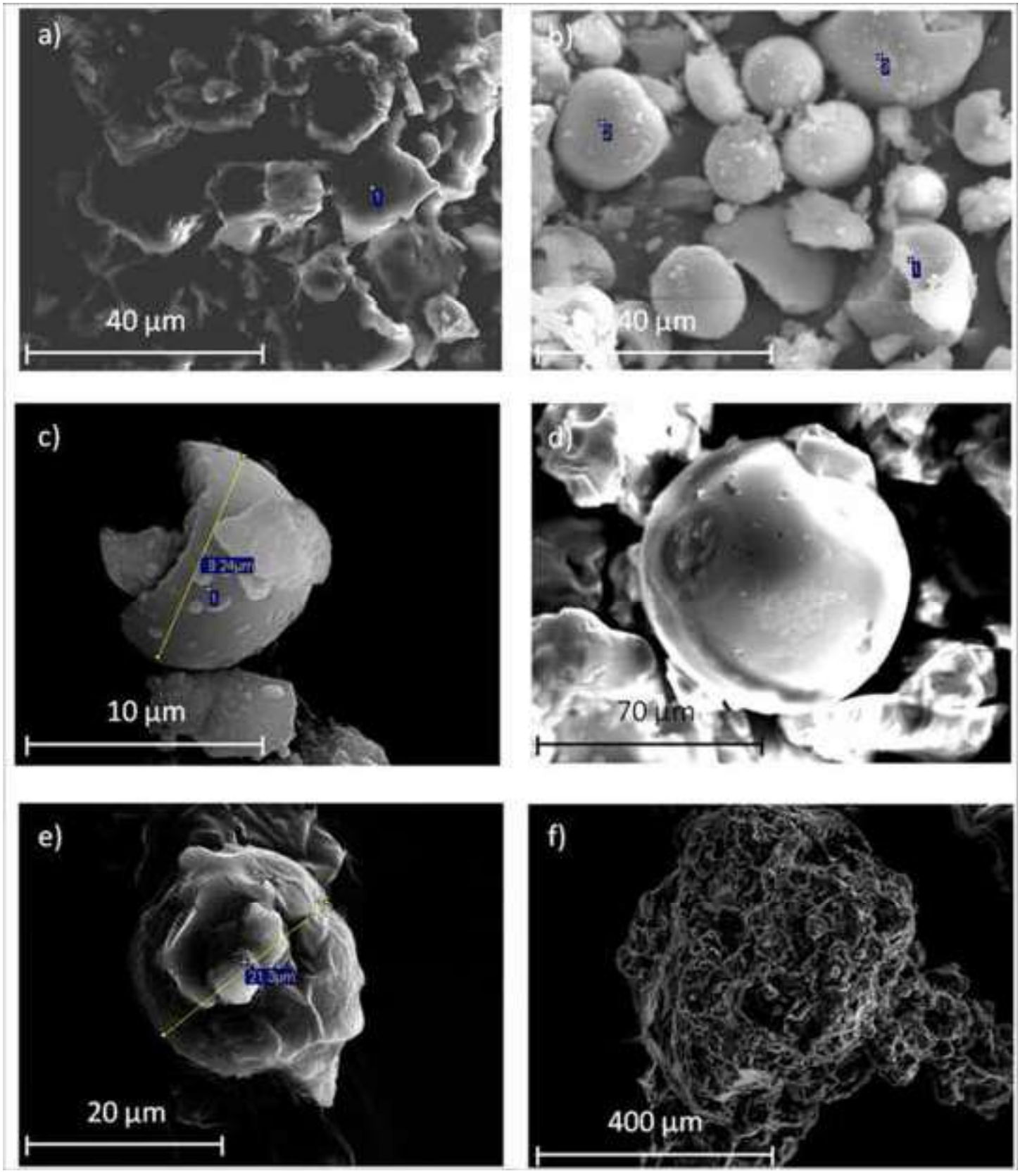

Figure 2

Click here to access/download;Figure;Figure 2.tif

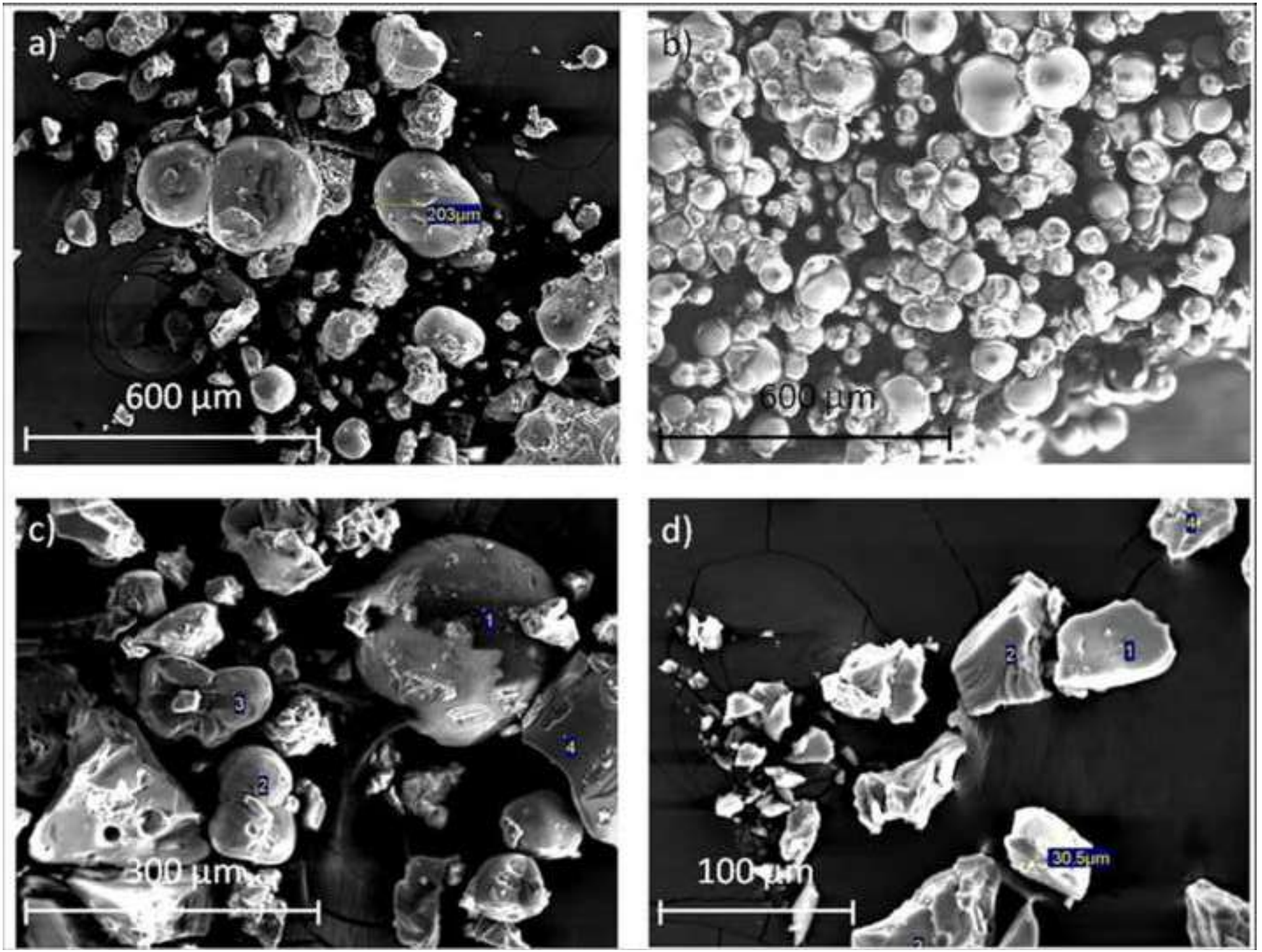

Figure 3

Click here to access/download;Figure;Figure 3.tif

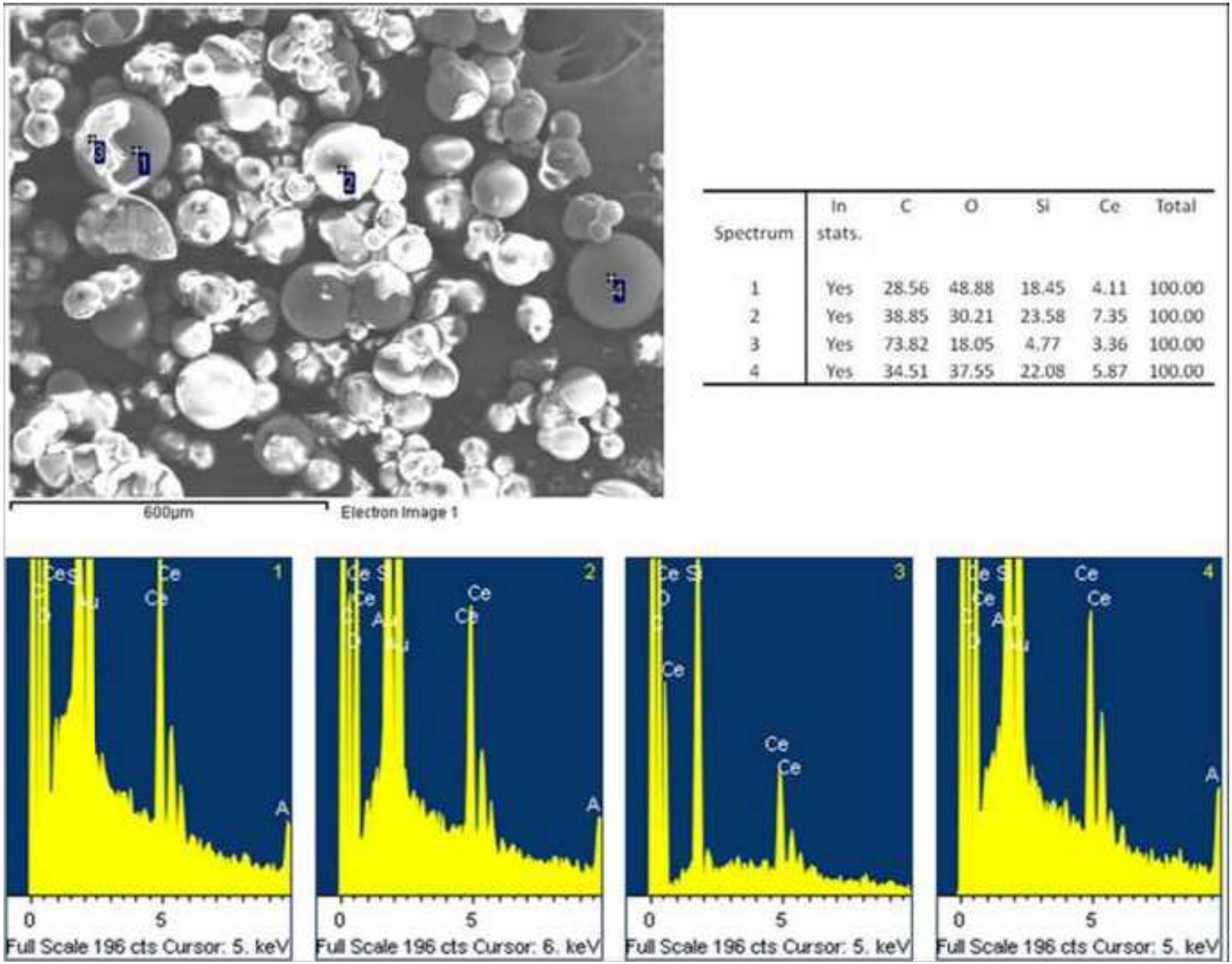

Spectrum	In stats.	C	O	Si	Ce	Total
1	Yes	28.56	48.88	18.45	4.11	100.00
2	Yes	38.85	30.21	23.58	7.35	100.00
3	Yes	73.82	18.05	4.77	3.36	100.00
4	Yes	34.51	37.55	22.08	5.87	100.00

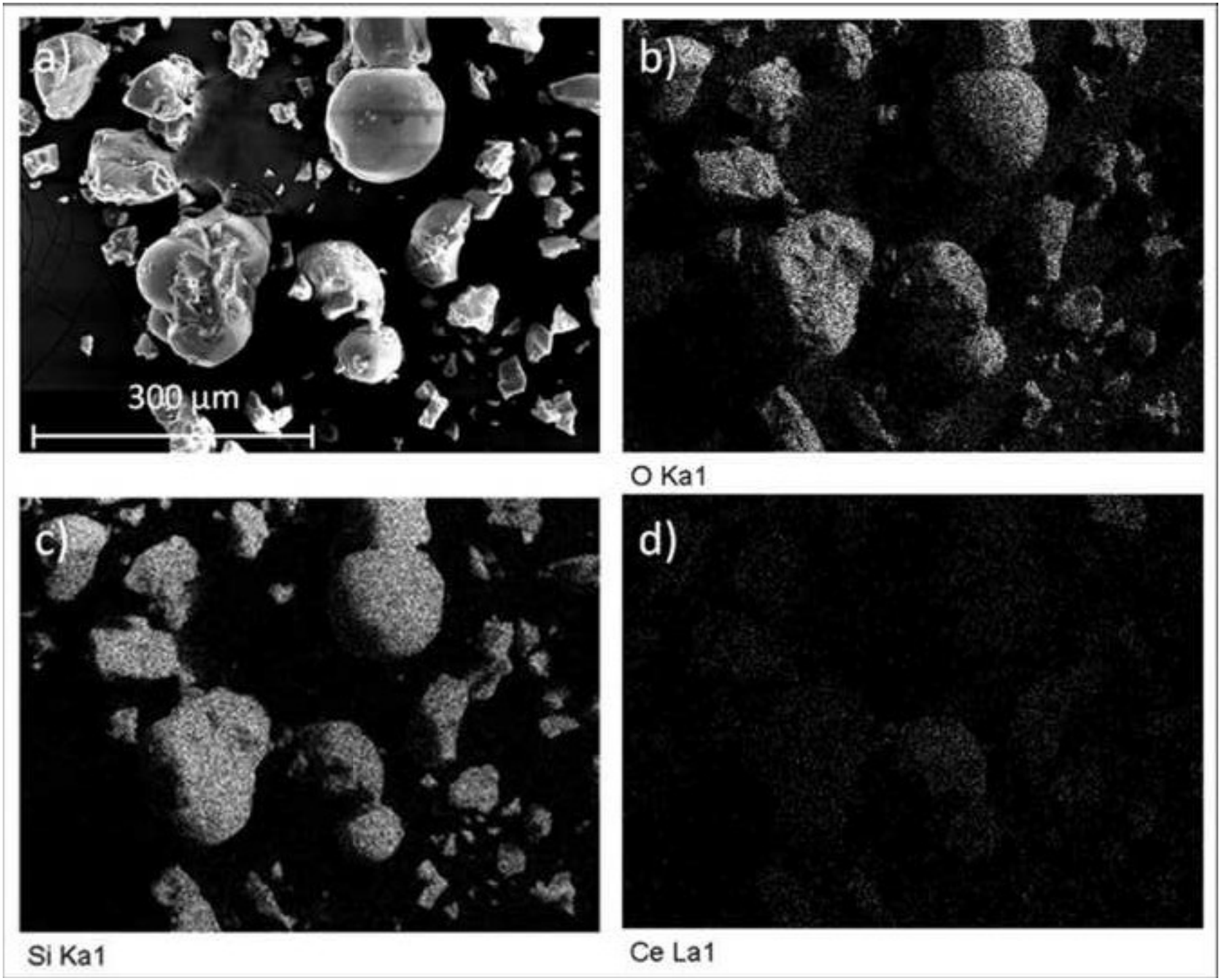

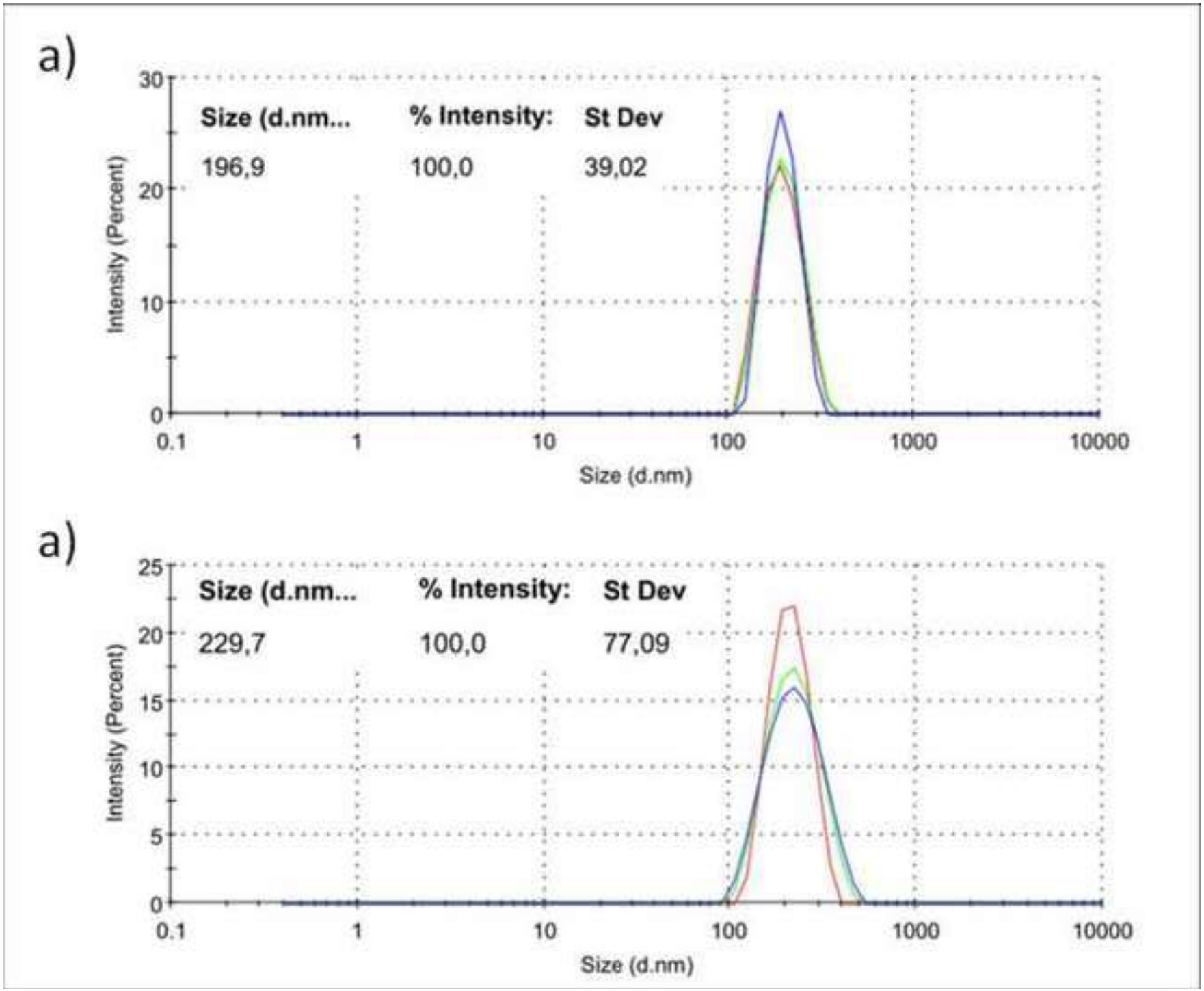

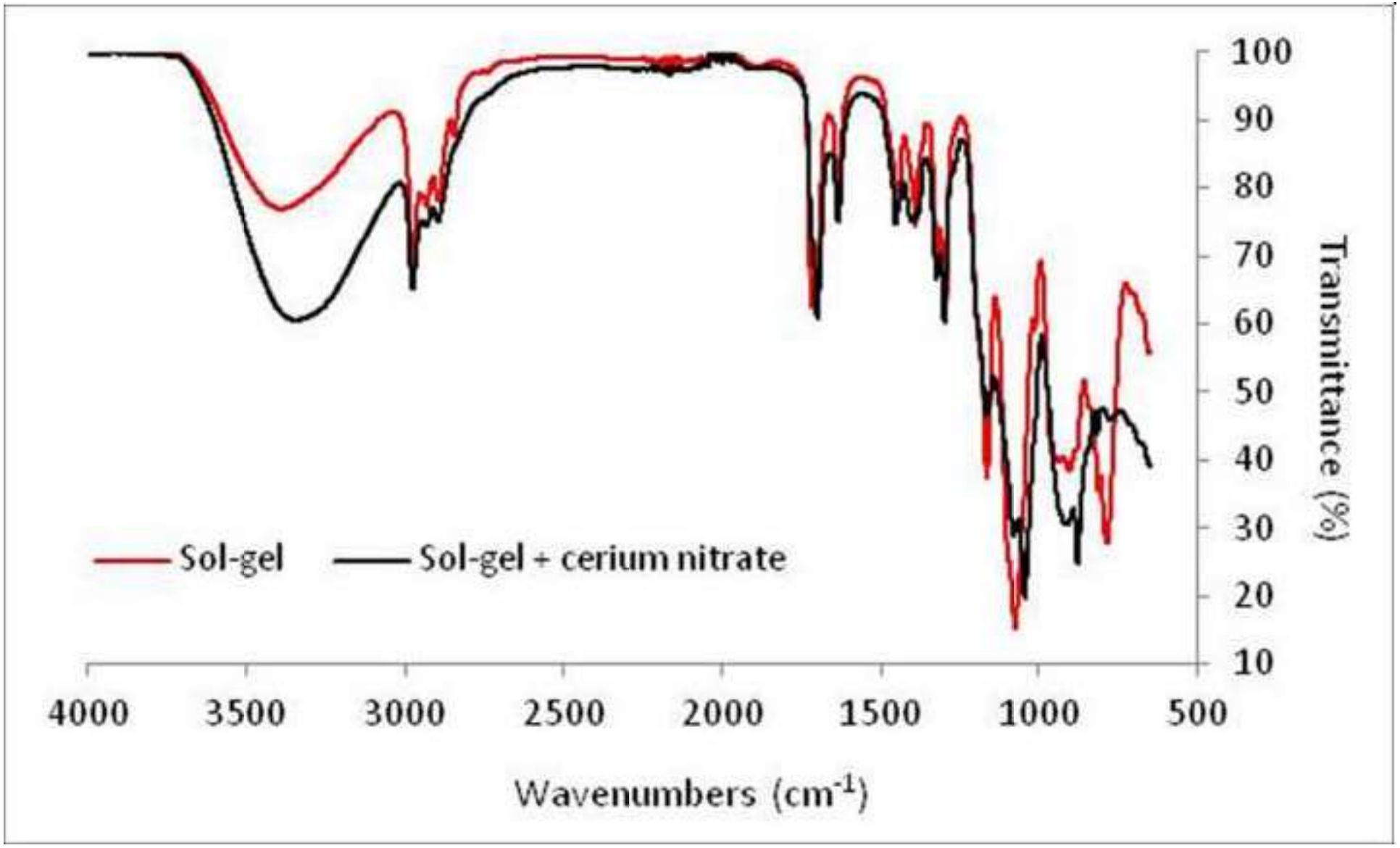

Figure 7

Click here to access/download;Figure;Figure 7.tif

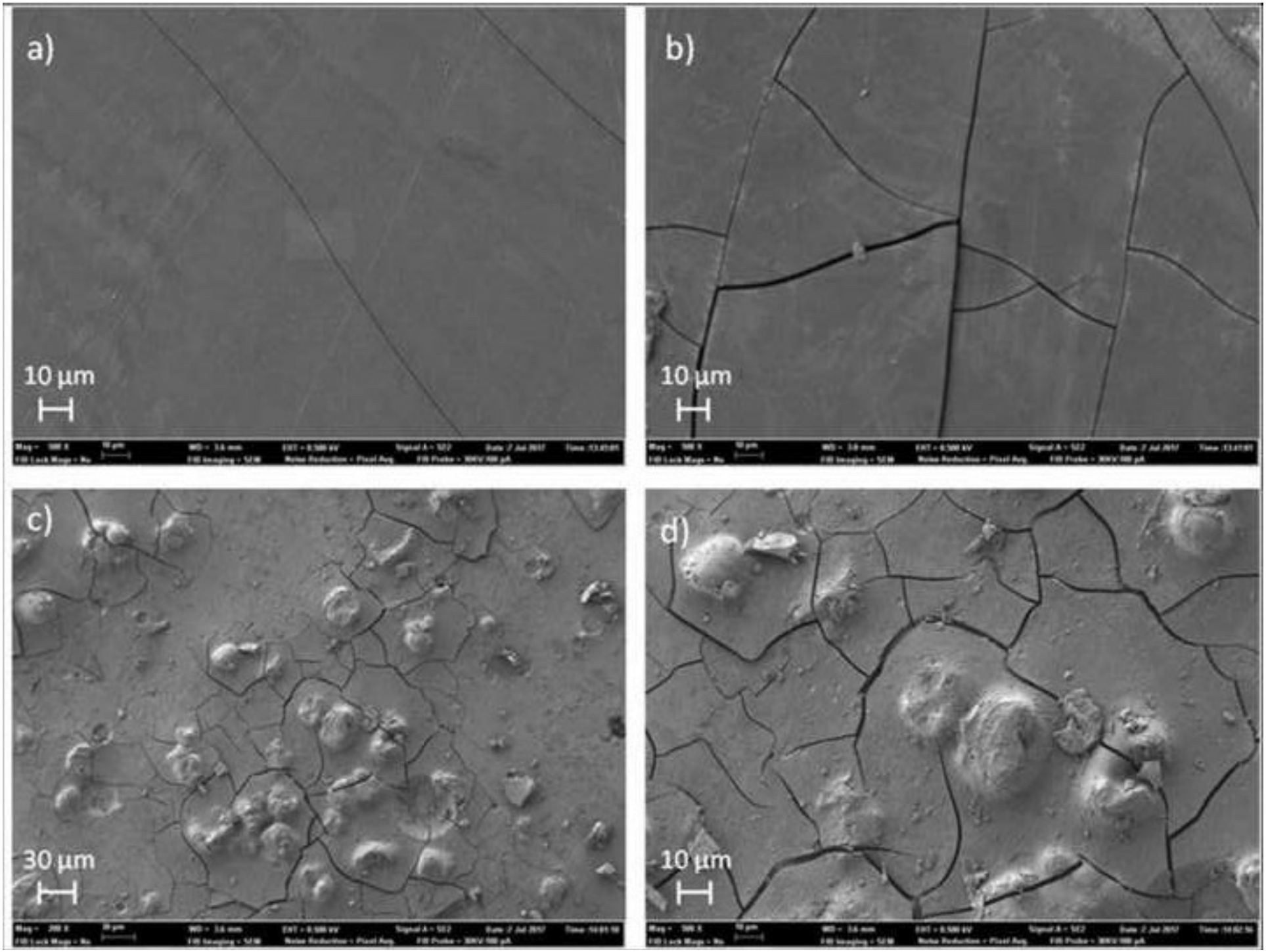

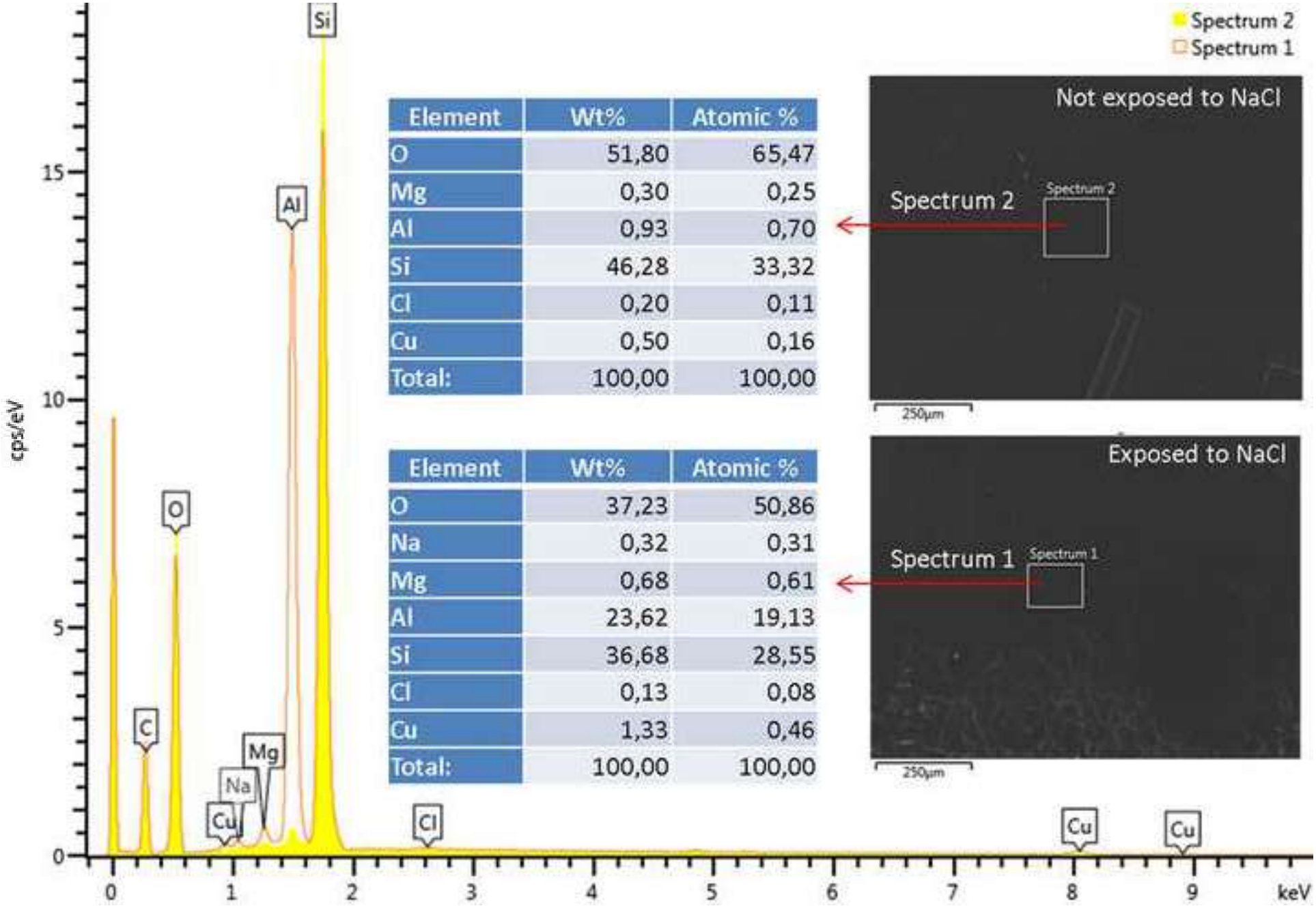

Element	Wt%	Atomic %
O	51,80	65,47
Mg	0,30	0,25
Al	0,93	0,70
Si	46,28	33,32
Cl	0,20	0,11
Cu	0,50	0,16
Total:	100,00	100,00

Element	Wt%	Atomic %
O	37,23	50,86
Na	0,32	0,31
Mg	0,68	0,61
Al	23,62	19,13
Si	36,68	28,55
Cl	0,13	0,08
Cu	1,33	0,46
Total:	100,00	100,00

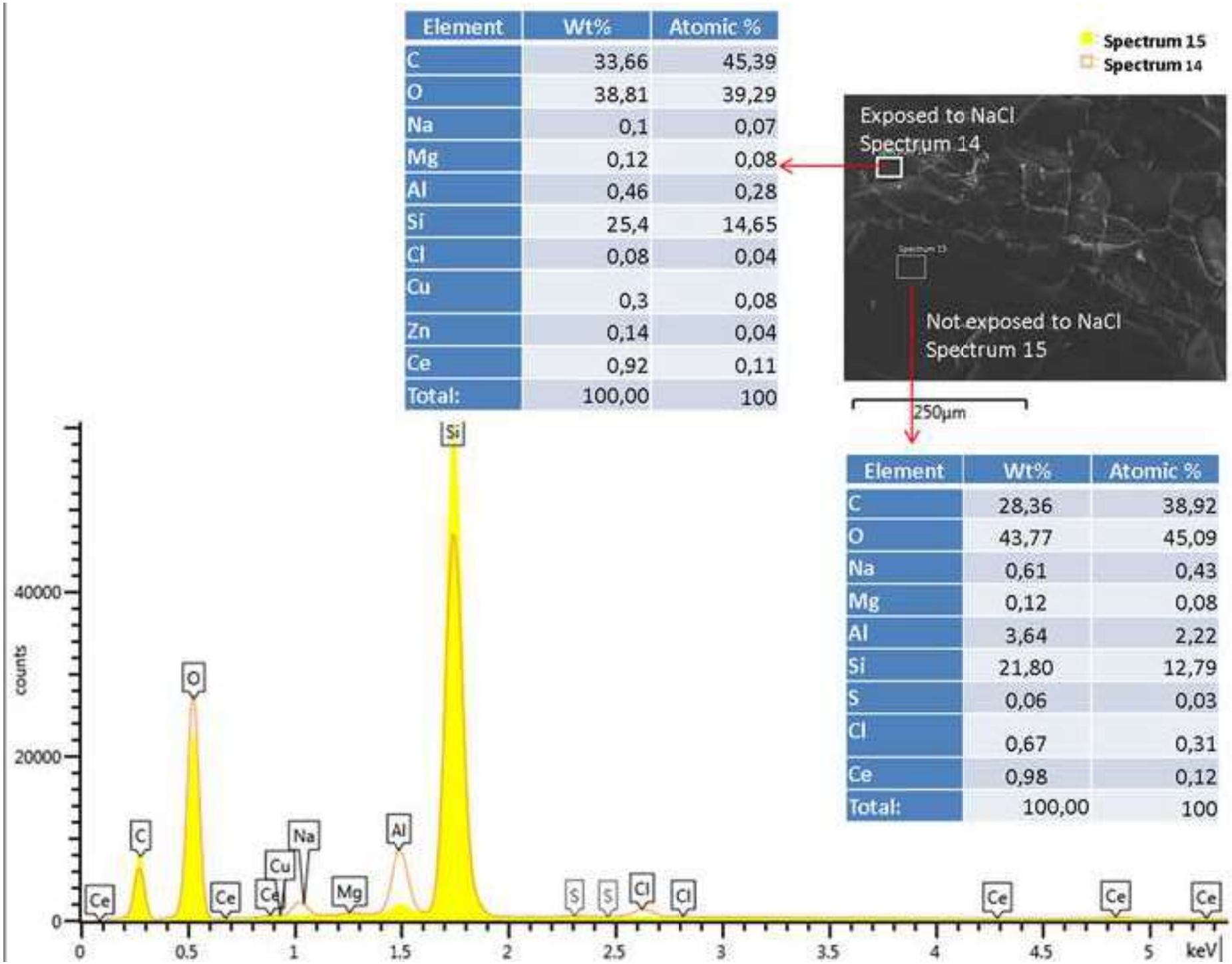

Element	Wt%	Atomic %
C	33,66	45,39
O	38,81	39,29
Na	0,1	0,07
Mg	0,12	0,08
Al	0,46	0,28
Si	25,4	14,65
Cl	0,08	0,04
Cu	0,3	0,08
Zn	0,14	0,04
Ce	0,92	0,11
Total:	100,00	100

Element	Wt%	Atomic %
C	28,36	38,92
O	43,77	45,09
Na	0,61	0,43
Mg	0,12	0,08
Al	3,64	2,22
Si	21,80	12,79
S	0,06	0,03
Cl	0,67	0,31
Ce	0,98	0,12
Total:	100,00	100

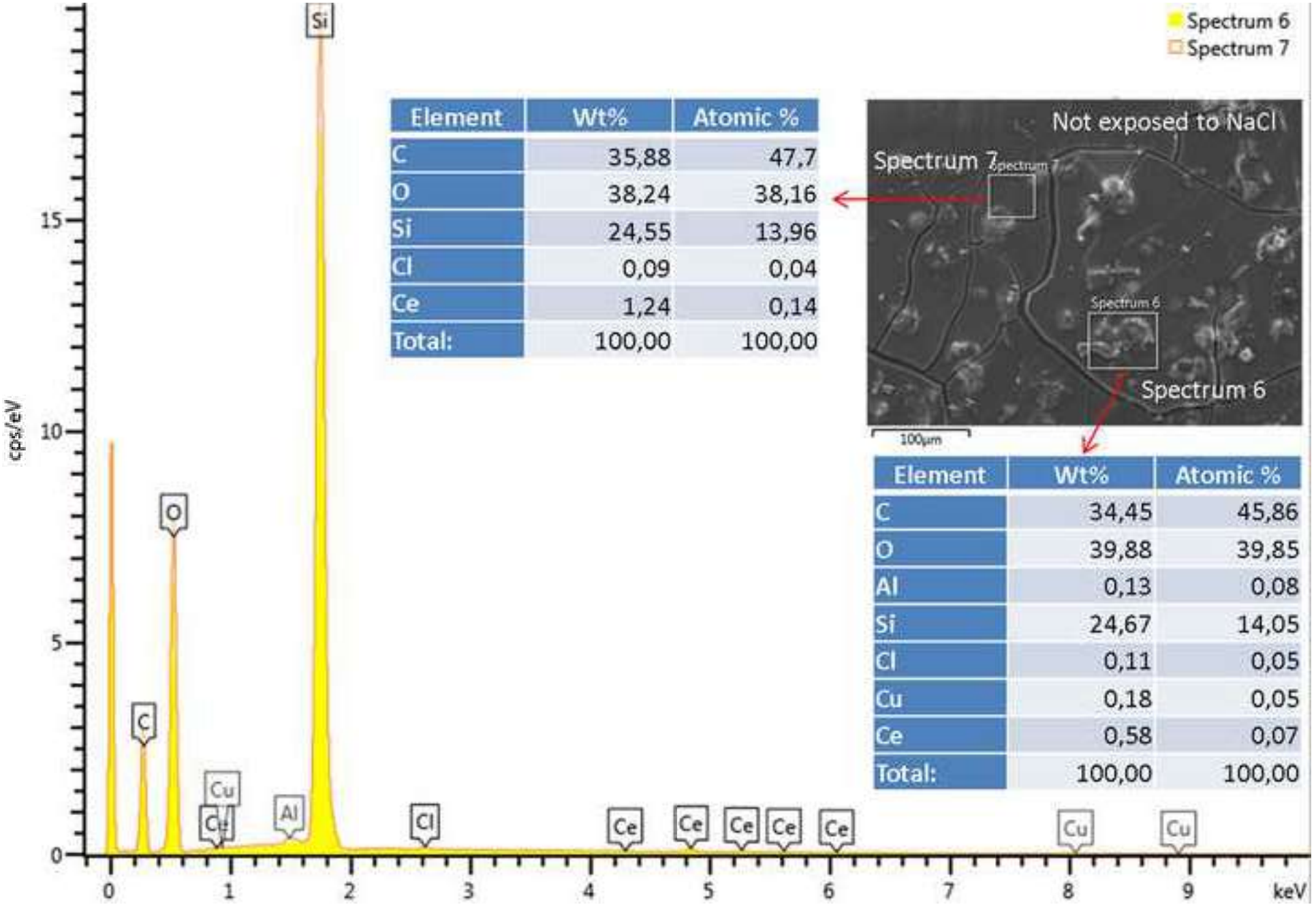

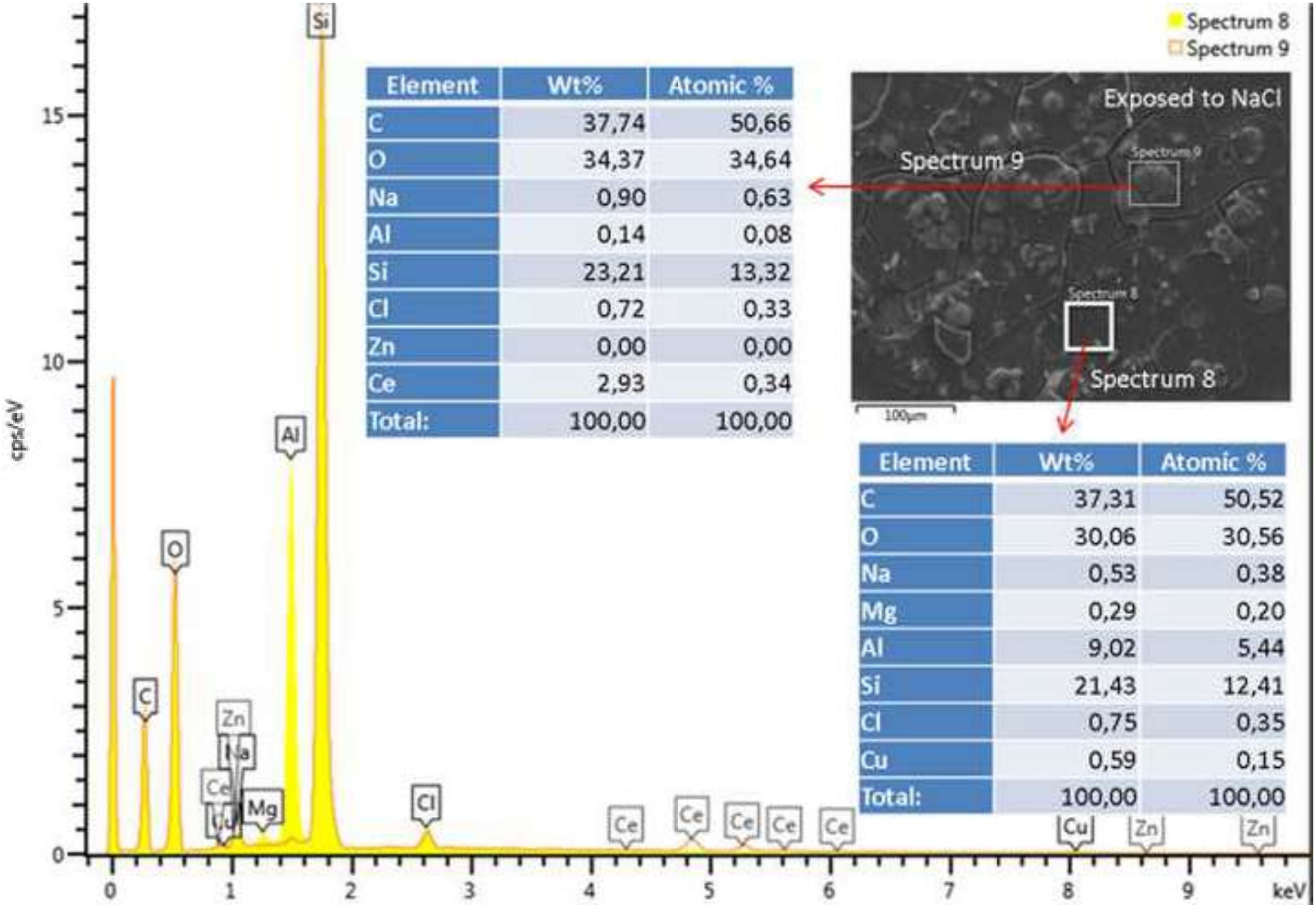

Element	Wt%	Atomic %
C	37,74	50,66
O	34,37	34,64
Na	0,90	0,63
Al	0,14	0,08
Si	23,21	13,32
Cl	0,72	0,33
Zn	0,00	0,00
Ce	2,93	0,34
Total:	100,00	100,00

Element	Wt%	Atomic %
C	37,31	50,52
O	30,06	30,56
Na	0,53	0,38
Mg	0,29	0,20
Al	9,02	5,44
Si	21,43	12,41
Cl	0,75	0,35
Cu	0,59	0,15
Total:	100,00	100,00

Figure 12

Click here to access/download;Figure;Figure 12.tif

a)

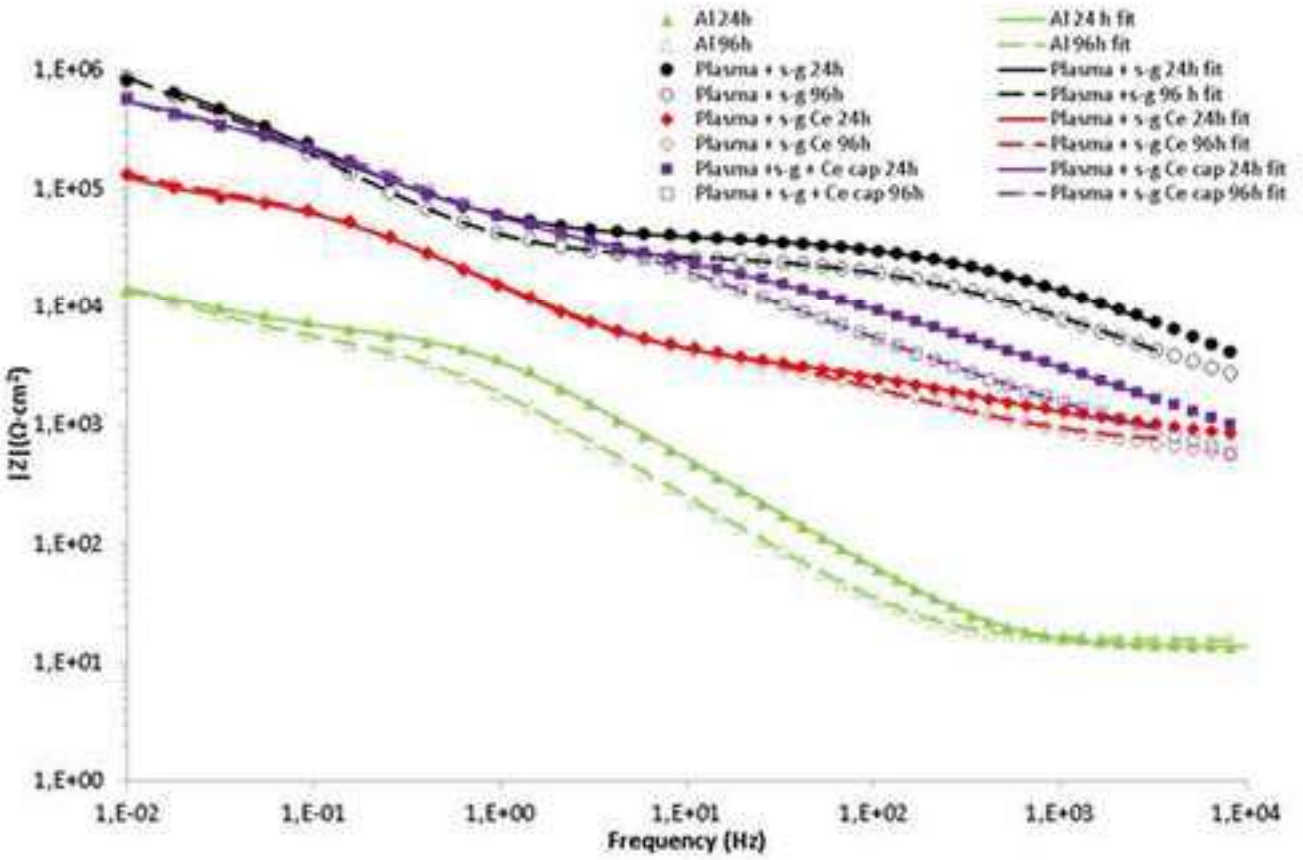

b)

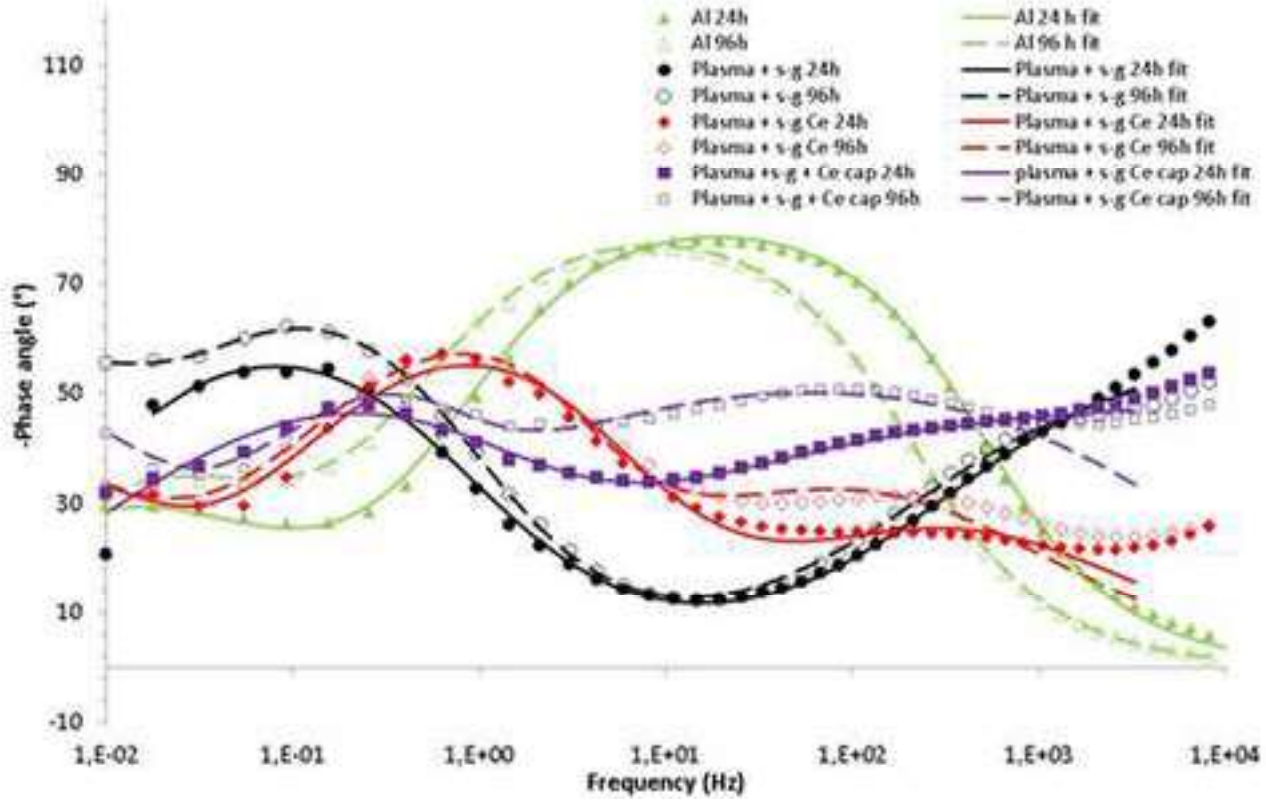

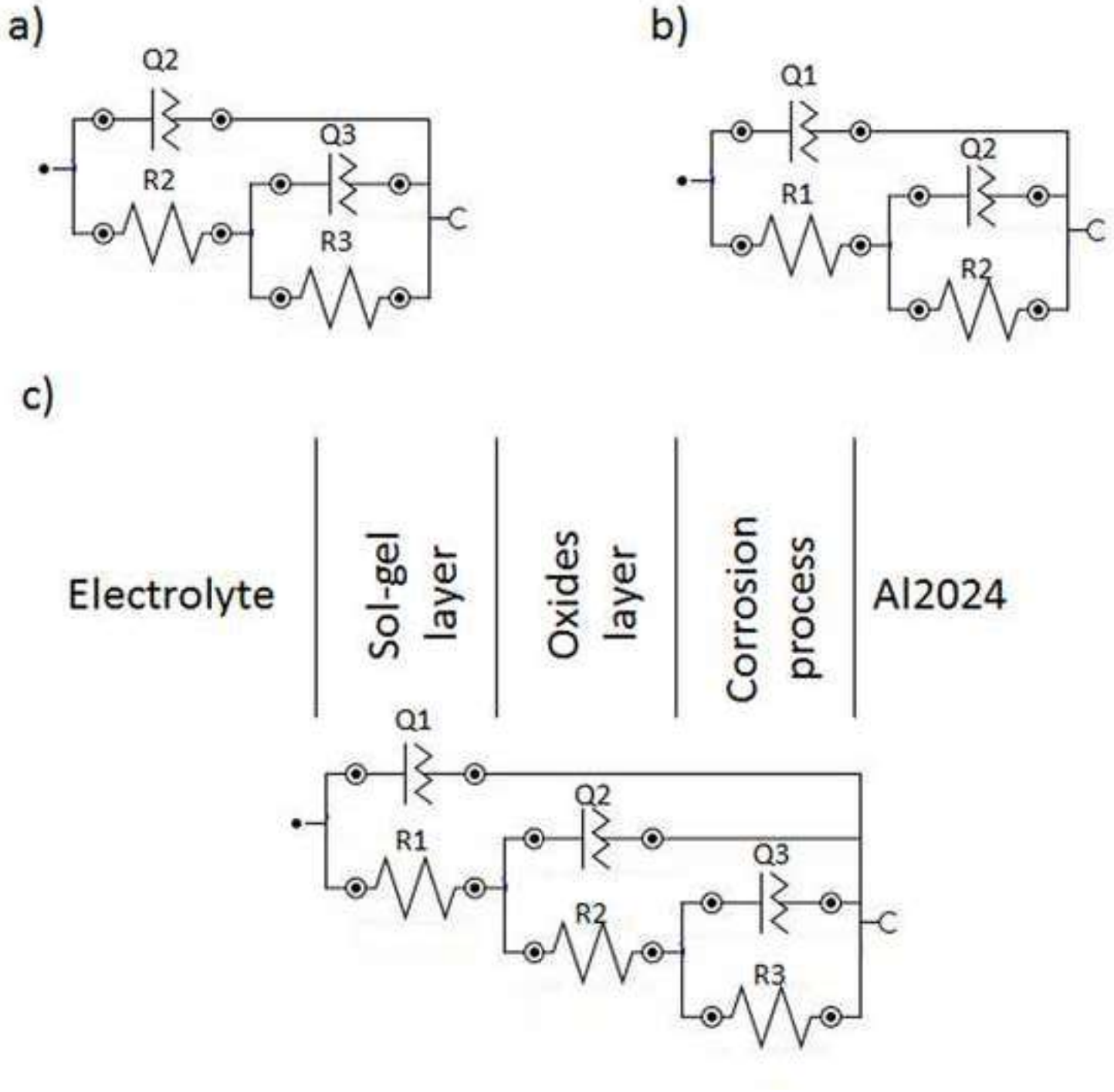

	Water phase				Oil phase		Catalyst
	$Ce(NO_3)_3$ (g)	Water (g)	Ethanol (g)	Span 80 (g)	sunflower-seed oil (g)	TEOS (ml)	2M HCl (ml)
A.1	3	5	5	0.92	46	15	0.05

Table 1. Formulation of $Ce(NO_3)_3$ microcapsules using acid catalyst.

	Water phase						Oil phase	Catalyst
	$Ce(NO_3)_3$ (g)	Water (g)	2M HCl (ml)	Ethanol (g)	TEOS (ml)	Span 80 (g)	sunflower-seed oil (g)	25 % NH_3 (ml)
B.1	3	5	0.05	5	15	0.92	46	2
B.2	3	10	0.05	0	15	0.92	46	2
B.3	3	3	0.05	8	15	0.92	46	2
B.4	3	5	0.05	5	15	2.3	46	2
B.5	3	10	0.05	0	15	2.3	46	2
B.6	3	3	0.05	8	15	2.3	46	2

Table 2. Formulations of $Ce(NO_3)_3$ microcapsules using basic catalyst.

Voltage (V)	Frequency (kHz)	Nozzle-sample distance (mm)	Nozzle velocity (m/min)	Ionization gas	Ionization gas flow rate (L/h)
90	21	5	10	Compressed air	2400

Table 3. Operational conditions employed in plasma activation of AA2024 surface.

Component	Formulation		
	SGA	**SGA + Ce**	**SGA + Ce microcapsules**
Ethanol	87.6 mL	87.6 mL	87.6 mL
TEOS	62.9 mL	62.9 mL	62.9 mL
MAPTMS	22.4 mL	22.4 mL	22.4 mL
Acid water (pH 1 with nitric acid)	27.1 mL	27.1 mL + 1.269 g $Ce(NO_3)_3$	27.1 mL + 4.097 g Cerium microcapsules
Total volume	200 mL	200 mL	200 mL

Table 4. Composition of the different sol-gel formulations used.

Route	Silica precursor (TEOS)	SEM (morphology)
A	In oil phase and acid catalyst	Microcapsules not formed
B	In aqueous phase and basic catalyst	Microcapsules formed

Table 5. Synthesis route and results depending on in which phase TEOS is located.

Sample	Aqueous phase			SEM morphology
	H_2O (g)	EtOH (g)	$Ce(NO_3)_3$	
B.4	5	5	3	Completely formed
B.5	10	0	3	Partially broken
B.6	3	8	3	Partially broken

Table 6. Morphology of the microcapsules observed by SEM in function of the $[H_2O]/[EtOH]$ molar ratio.

Sample	Oil phase		Size distribution by SEM
	Seeds oil (g)	Span 80 (g)	
B.4	46	2.5	Homogenous
B.1	46	1	Heterogeneous

Table 7. Size distribution of the microcapsules (observed by SEM) using different concentration of surfactant span 80.

Sample	Temperature of drying (ºC)	Morphology (SEM)
B4-25	25	Spherical, not damaged
B4-40	40	Spherical, some damaged
B4-70	70	Spherical, completely damaged

Table 8. Morphology of the microcapsules depending on the drying temperature applied.

Table 9. Values of impedance modulus |Z| at 0.01 Hz for the different samples analyzed by means of EIS.

	$\|Z\|$ ($\Omega \cdot cm^2$)	
Sample	24 h	96 h
Al	$1.4 \cdot 10^4$	$1.4 \cdot 10^4$
Al + plasma + sol-gel	$8.1 \cdot 10^5$	$8.7 \cdot 10^5$
Al + plasma + sol-gel + Cerium	$1.3 \cdot 10^5$	$1.4 \cdot 10^5$
Al + plasma + sol-gel + encapsulated Cerium	$5.6 \cdot 10^5$	$5.9 \cdot 10^5$

Table 10. Fitted parameters according to electrochemical equivalent circuits presented in Fig. 13.

		Samples							
		Al 24h	**Al 96h**	**s-g 24h**	**s-g 96h**	**s-g Ce 24h**	**s-g Ce 96h**	**s-g Ce cap 24h**	**s-g Ce cap 96h**
Q1	**Y1 (µMho*s^N)**	-	-	0,169	0,364	5,49	9,61	2,87	3,54
	N1	-	-	0,666	0,642	0,627	0,625	0,537	0,616
R1	**R1 (kΩ)**	-	-	40	28,6	3,63	6,5	52,7	127
Q2	**Y2 (µMho*s^N)**	40	87,2	6,7	7,4	10,4	6,87	3,62	2,06
	N2	0,932	0,923	0,783	0,873	0,854	0,958	0,742	1,0
R2	**R2 (kΩ)**	6,03	5,25	1660	1190	108	124	950	494
Q3	**Y3 (µMho*s^N)**	530	544	-	16,1	193	161	-	39,9
	N3	0,689	0,745	-	1,0	0,964	0,936	-	1,0
R3	**R3 (kΩ)**	26,9	21,3	-	2320	206	250	-	1200
χ^2		0,029802	0,0054978	0,0152	0,022096	0,085689	0,23608	0,02199	0,12755